Pairwise annihilation of Weyl nodes induced by magnetic fields in the Hofstadter regime

Faruk Abdulla*

Harish-Chandra Research Institute, A CI of Homi Bhabha National Institute, Chhatnag Road, Jhunsi, Prayagraj (Allahabad) 211019, India and Physics Department, Technion - Israel Institute of Technology, Haifa 32000, Israel

(Received 30 January 2024; accepted 4 April 2024; published 15 April 2024)

Weyl semimetal, which does not require any symmetry except translation for protection, is a robust gapless state of quantum matter in three dimensions. When translation symmetry is preserved, the only way to destroy a Weyl semimetal state is to bring two Weyl nodes of opposite chirality close to each other to annihilate pairwise. An external magnetic field can destroy a pair of Weyl nodes (which are separated by a momentum space distance $2k_0$) of opposite chirality, when the magnetic length l_B becomes close to or smaller than the inverse separation $1/2k_0$. In this work, we investigate pairwise annihilation of Weyl nodes induced by an external magnetic field which ranges from a small to a very large value in the Hofstadter regime. We show that this pairwise annihilation in a Weyl semimetal featuring two Weyl nodes leads to the emergence of either a normal insulator or a layered Chern insulator. In the case of a Weyl semimetal with multiple Weyl nodes, the potential for generating a variety of states through external magnetic fields emerges. Our study introduces a straightforward and intuitive representation of the pairwise annihilation process induced by magnetic fields, enabling accurate predictions of the phases that may appear after pairwise annihilation of Weyl nodes.

DOI: 10.1103/PhysRevB.109.155142

I. INTRODUCTION

Weyl semimetals (WSMs) [1–10] are examples of three-dimensional topological semimetals where nondegenerate valence and conduction bands touch at an even number of isolated points in the 3D Brillouin zone (BZ) called Weyl nodes (WNs). Each WN carries a topological charge and has a definite chirality. The fact that WNs carry nontrivial topological charges leads to existence of special kind of surface states called surface Fermi arc which joins the projections of WNs of opposite chiralities onto the surface Brillouin zone (SBZ).

Weyl semimetal is a robust topological state of quantum matter. When spatial translation symmetry is preserved, the only way to destroy the state is to bring two WNs of opposite chiralities (or topological charges) close to each other to annihilate them pairwise [1]. Weyl semimetals which are known for many exotic properties such as chiral anomaly [11–13], negative magnetoresistance [14–21], planar Hall effect [22–26], and Fermi arc mediated quantum oscillations and 3D quantum Hall effect [27–36], require a presence of external magnetic fields to exhibit the above mentioned properties. However, an external magnetic field, if strong enough, can couple a pair of WNs of opposite chirality and can potentially annihilate them to destroy the WSM state. The authors in Refs. [37,38] found that pairwise annihilation of WNs by external magnetic field can happen when the inverse magnetic length $l_B^{-1} = \sqrt{eB/\hbar}$ becomes close to or larger than the momentum space separation $2k_0$ between the two WNs of opposite chirality.

To investigate the pairwise annihilation of WNs induced by external magnetic fields, the authors in Refs. [37,38] considered a simple model of WSM, with two WNs only, in a continuum approximation. A Hamiltonian with two WNs located at $\mathbf{k}_w = (k_0, 0, 0)$ and $-\mathbf{k}_w$ may be approximated in a continuum as

$$H_{\rm con}(\mathbf{k}) = \left(k_0^2 - k_x^2\right)\sigma_x + k_y\sigma_y + k_z\sigma_z. \tag{1}$$

The WNs are separated along the k_x axis and the distance is $2k_0$ in momentum space. Pairwise annihilation of Weyl nodes which causes a transition from gapless semimetal to an insulator, has been also observed in the experiments by measuring the resistivity of Weyl materials TaP [39] and TaAs [40] at a high applied magnetic fields.

Working with the low-energy continuum Hamiltonian outlined in Eq. (1) for a WSM presents several limitations. Firstly, the applicability of the continuum Hamiltonian in Eq. (1), derived from the full lattice model of a WSM, is constrained to situations where the separation $2k_0$ between the two Weyl nodes is relatively small. Secondly, when dealing with strong magnetic fields in the regime where the magnetic length l_B is comparable to the lattice constant denoted as a (Hofstadter regime), any continuum approximation of the complete lattice model exceeds its range of relevance. The efficacy of the low energy continuum Hamiltonian in Eq. (1) for a WSM with two Weyl nodes is confined to the conditions: $\ell_B \gg a$ and $1/2k_0 \gg a$.

The preceding discussion underscores the increasing complexity associated with investigating pairwise annihilation of WNs within a continuum model of WSMs featuring multiple WNs (e.g., time-reversal preserved WSMs), especially when multiple node separations are involved. Another crucial constraint is that a continuum model cannot anticipate the subsequent state following the pairwise annihilation of Weyl nodes. This process may yield not only normal insulating states but also states with nontrivial topological characteristics.

*farukhrim@gmail.com

Addressing the aforementioned challenges can be achieved by exploring a lattice model of a WSM to investigate the pairwise annihilation of WNs induced by external magnetic fields. The authors in Ref. [41], among other things, offered valuable insights into this direction. In their work, they specifically examined a complicated lattice model of a time-reversal broken WSM which involves many parameters, with a primary emphasis on constructing phase diagrams in the presence of commensurate magnetic fields. Their findings revealed new phases which include layered Chern insulator (LCI), insulator which is trivial in the bulk but has counter propagating surface states on certain open surface (I′), and a coexistent phase (W2′) where Chern bands and WPs coexist with their own Fermi arc surface states. The emergence of these diverse phases from a given WSM state was not immediately apparent.

In examining the pairwise annihilation WNs, it is essential to recognize that an external magnetic field, aligned with the direction of separation between two WNs of opposite chirality, cannot couple these two nodes. The possibility of pairwise annihilation by an external field arises only when the field is not parallel to the direction of separation between two WNs of opposite chirality. To streamline the computation without sacrificing the essence of the problem, we will presume that the external magnetic field's direction is perpendicular to the separation between two Weyl nodes of opposite chirality.

In this work, first, we consider a simple model of time-reversal broken WSM with only one parameter k_0 ($2k_0$ is the separation between two WNs in the momentum space) to understand how the pairwise annihilation of WNs induced by external magnetic fields can lead to different states. We show that the pairwise annihilation in a WSM with two WNs leads to either a normal insulator (no surface states) or a layered Chern insulator. Then based on the concept that a pair of WNs (separated by $2k_0$) gets annihilated when $l_B \sim 1/2k_0$, we develop a model independent intuitive representation of pairwise annihilation process (an example in Fig. 1) induced by external magnetic fields. Importantly, this intuitive picture of pairwise annihilation only requires information about the Weyl nodes' locations and the connectivities of Fermi arcs in the surface BZ to accurately predict the phases which can appear after pairwise annihilation of Weyl nodes. We apply the intuitive picture of pairwise annihilation to demonstrate how the states like LCI, I′ and W2′ can be straightforwardly obtained from a simpler WSM state, without resorting to any complicated model as was considered by Ref. [41].

Second, we consider a minimal model of time-reversal preserved WSM with four Weyl nodes. The minimal model with four WNs has two free parameters k_1 and k_2 which provide momentum space separation between Weyl nodes of opposite chirality. In a WSM with four WNs, there are three distinct perpendicular directions in which a magnetic field can be applied to induce pairwise annihilation of Weyl nodes. We meticulously construct phase diagrams for each of the three cases by solving the model with thorough effort. Subsequently, we assert that these phase diagrams can be easily derived from the intuitive representation of pairwise annihilation of WNs, requiring only minimal information about the WNs' locations and the connectivities of Fermi arcs on the surface BZ.

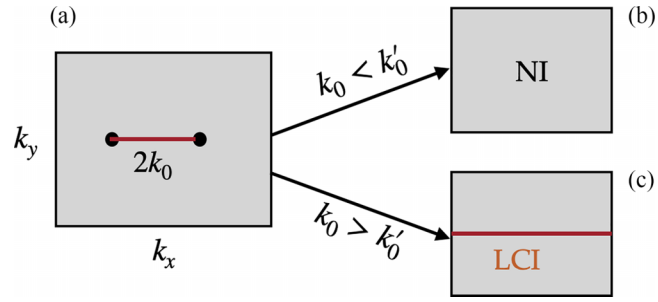

FIG. 1. An intuitive picture of how and when a normal insulator (NI) and a LCI state appear after pairwise annihilation of two WNs separated by a momentum space distance $2k_0$. (a) shows projections of the WNs (black dots) and the Fermi arc in the k_x-k_y surface BZ. The parameter $2k_0' = 2\pi - 2k_0$ measure the inter-BZ separation between the two WNs of opposite chirality. Two Weyl nodes get pairwise annihilated by magnetic field when the inverse magnetic length l_B^{-1} becomes close to or larger then momentum space separation between them. There are two scenarios prevail. When $k_0 < k_0'$, the inverse magnetic length l_B^{-1} first reaches the intra-BZ separation $2k_0$. In this case, when the magnetic field is increased, two WNs approach each other along the Fermi arc to meet at a point inside the BZ. This leads annihilation of the two nodes without leaving the Fermi arc. Hence a normal insulator emerges. On the other hand, if $k_0 > k_0'$, pairwise annihilation occurs at the boundary of the BZ by leaving the Fermi arc as depicted in (c). Hence a LCI state emerges.

We also touched upon pairwise annihilation of WNs induced by magnetic fields in a WSM with six Weyl nodes. We analyze a simple case where all the WNs are located in a single plane. The intuitive picture of pairwise annihilation of WNs immediately predicts emergence of two new coexistence phases.

The plan of the paper is as follows. In Sec. II, we conduct a thorough examination of pairwise annihilation of WNs by external magnetic fields in a simple model of WSM with two Weyl nodes (time-reversal broken case). Then in Sec. III, we study the pairwise annihilation in a minimal model of time-reversal preserved WSM with four WNs, which has two free parameters—the separations between WNs of opposite chirality. We discuss our findings in Sec. IV and summarize them in Sec. V. In Appendix, we discuss about nature of the insulating states which appear after pairwise annihilation of WNs in the time-reversal preserved model.

II. TIME-REVERSAL BROKEN WSM

We consider the following lattice model of time-reversal broken Weyl semimetal:

$$H(\mathbf{k}) = (2 + \cos k_0 - \cos k_x - \cos k_y - \cos k_z)\sigma_x + \sin k_y \sigma_y + \sin k_z \sigma_z \tag{2}$$

with minimal two WNs at $\mathbf{k}_w = (k_0, 0, 0)$ and $-\mathbf{k}_w$ carrying monopole charges $C = 1$ and -1, respectively. The two WNs are separated along the k_x axis by $2k_0$ and the parameter k_0 lies in the range $0 \leqslant k_0 \leqslant \pi$. It is easily checked that the Hamiltonian respects neither time-reversal or particle-hole symmetry. However, the Hamiltonian is symmetric under space inversion $\mathcal{P}H(\mathbf{k})\mathcal{P}^{-1} = H(-\mathbf{k})$, with $\mathcal{P} = \sigma_x$. Because of this inversion

symmetry and mirror about the yz plane, the Fermi arc which exist on k_x-k_y and k_x-k_z surface BZs is a straight arc joining the projections of the two Weyl points [see Fig. 1(a)].

We want to investigate pairwise annihilation of WNs by external magnetic fields for field's strength which ranges all the way from small ($\ell_B \gg a$) to a very large value ($\ell_B \sim a$) in the Hofstadter regime. Our goal is to identify the states that emerge following the pairwise annihilation of Weyl nodes. We know for sure that the pairwise annihilation in a WSM with two WNs always leads to insulating states. The question we are asking is what is the nature of these insulating states. Specifically, we seek to determine whether the insulator exhibits surface states and whether it possesses topological nontriviality.

As outlined in the previous section, the applied magnetic field which is not aligned along the direction of separation of two WNs of opposite chirality can couple the nodes and hence can potentially annihilate them. In our model (2), the Weyl nodes are separated along the k_x axis. To simplify the analysis, we assume the magnetic field is aligned perpendicular to the x axis, specifically aligned with the z axis. For a WSM with two WNs separated along the k_x direction, pairwise annihilation induced by magnetic field applied along either the z or y direction would result in identical sets of phases.

A. Hofstadter Hamiltonian and gapless solutions

An external magnetic field can be easily coupled to the Hamiltonian in Eq. (2) by taking it to the real space,

$$H = \sum_{\mathbf{n},j} c^\dagger(\mathbf{n}) 2M\sigma_x c(\mathbf{n}) - (c^\dagger(\mathbf{n} + a\hat{e}_j)\, T_j\, c(\mathbf{n}) + \text{H.c.}) \tag{3}$$

where $\mathbf{n} = a(n_x, n_y, n_z)$, n_i being integers, denote the lattice sites, $\hat{e}_j$ is the unit vector along jth direction, and $M = 2 + \cos k_0$. The hopping matrices T_j, $j = (x, y, z)$, are given by $T_x = \sigma_x$, $T_y = \sigma_x + i\sigma_y$ and $T_z = \sigma_x + i\sigma_z$. The lattice constant a is set to be unity for the rest of the paper.

In presence of an external magnetic fields, the hopping terms in the Hamiltonian Eq. (3) pick up a nontrivial phase factor under Peierls substitution [42]. For a uniform magnetic field aligned in the z-direction $\mathbf{B} = B\hat{z}$, we can choose to work in the Landau gauge $\mathbf{A} = (-y, 0, 0)B$, where only the hopping in the x direction picks up a nontrivial phase so that the Hamiltonian in a magnetic field is obtained from Eq. (3) by the replacement $T_x \to \exp(-i2\pi y\phi/\phi_0)T_x$. We restrict ourselves to the case where the flux ϕ (in units of the magnetic flux quantum $\phi_0 = h/e$) per unit cell is commensurate, i.e., $\phi/\phi_0 = Ba^2/\phi_0 = p/q$, where p and q are relatively prime, so that translation symmetry along the y direction is restored with a larger unit cell [43]. In order to diagonalize the Hamiltonian, we introduce a magnetic unit cell that expands q times in comparison to the original unit cell, elongating along the y direction. Employing Fourier transformation in relation to the Bravais lattice positions within the magnetic unit cell yields following Hofstadter Hamiltonian:

$$H_\phi = \sum_{\alpha=0}^{q-1} c^\dagger_\alpha(\mathbf{k})\left[f_1^\alpha(\mathbf{k})\sigma_x + f_3^\alpha(\mathbf{k})\sigma_z\right]c_\alpha(\mathbf{k}) - (c^\dagger_{[\alpha+1]}(\mathbf{k})e^{iqk_y\delta_{(\alpha,q-1)}}\, T_y\, c_\alpha(\mathbf{k}) + \text{H.c.}), \tag{4}$$

where $\alpha = 0, 1, \ldots, q-1$ are the sublattice indices in the magnetic unit cell and $\mathbf{k}$ lies in the reduced (magnetic) Brillouin zone (MBZ), i.e., $\mathbf{k}$: $k_x \in (0, 2\pi)$, $k_y \in (0, 2\pi/q)$, $k_z \in (0, 2\pi)$. The square bracket notation in $c^\dagger_{[\alpha+1]}(\mathbf{k})$ implies that the values of α are taken modulo q - *i.e.*, $[\alpha] = \alpha \mod q$. The functions f_1^α and f_3^α are

$$f_1^\alpha(\mathbf{k}) = 2\left(M - \cos\left(k_x + \frac{2\pi p}{q}\alpha\right) - \cos k_z\right), \tag{5a}$$

$$f_3^\alpha(\mathbf{k}) = f_3(\mathbf{k}) = 2\sin k_z. \tag{5b}$$

Note that there is only one free parameter k_0 (enters through $M = 2 + \cos k_0$) which determines the separation between the two WNs of opposite chirality in our zero field model. Our goal is to determine the phase diagram for different values of p/q. The phase diagrams can be constructed if we can find all the gapless points (band touching points) of the Hofstadter Hamiltonian H_ϕ.

It is typically not possible to analytically determine the full energy spectrum of a Hofstadter Hamiltonian for all combinations of p and q values. However in some special cases, all the zeros (gapless solutions) of a Hofstadter Hamiltonian can be found for different values of p and q. Following Ref. [41], we find the energy spectrum of H_ϕ

$$E_n(\mathbf{k}) = \pm\sqrt{\gamma_n(\mathbf{k}, p, q) + (f_3(\mathbf{k}))^2}, \tag{6}$$

which is symmetric about the zero energy, $n = 1, 2, \ldots, q$, is the Landau level index and $\gamma_n(\mathbf{k}, p, q) \geqslant 0$ for all $\mathbf{k}$, p and q. Clearly the zero energy solutions are given by $f_3(\mathbf{k}) = 2\sin k_z = 0$ and $\gamma_1(\mathbf{k}, p, q) = 0$. The first condition tells that band touching along the k_z direction can occur only at $k_z = 0$ and/or π. Though the quantity $\gamma_1(\mathbf{k}, p, q)$ is not known explicitly (as a function of $\mathbf{k}$, p and q), $\gamma_1(\mathbf{k}, p, q) = 0$ can be solved exactly for all $\mathbf{k}$, p and q values. Solving $\gamma_1(\mathbf{k}, p, q) = 0$, we find band touching along the k_y and k_z directions can happen only at $k_y = 0$ and 0, respectively. We notice that the external magnetic field (aligned along the z direction) did not alter the band touching points along the k_y and k_z directions, i.e., the touching point remains at $k_y = k_z = 0$. The corresponding k_x values are given by [41]

$$\cos qk_x = (-1)^p[-T_q(g) + 2^{q-1}], \tag{7}$$

where $g = 1 + \cos k_0$ and $T_q(g)$ is a Chebyshev polynomial of degree q of first kind. The gapless solutions (exists only when the right-hand side of Eq. (7) lies in the range $[-1, 1]$) describes isolated point touchings which are the Weyl nodes in the theory. The WNs remain separated along the k_x direction. Note that though the integer p of flux p/q can change the sign of the right-hand side of Eq. (7), it does not affect the region of gapless solutions and hence the phase diagrams. In what follows, we will assume $p = 1$, unless it is stated.

The region where Eq. (7) exhibits a continuous solution (gapless solution) for various flux values is illustrated in Fig. 2. As the flux $1/q$ varies, the system transitions between gapped and gapless states for both small and large values of k_0. This process of gapping out the WNs can be elucidated as follows. Initially, at zero field, the two WNs are situated at $k_x = \pm k_0$ along the k_x axis. Upon introducing a magnetic field, the new positions of these WNs within the magnetic BZ are determined by the solutions of Eq. (7). With an increase

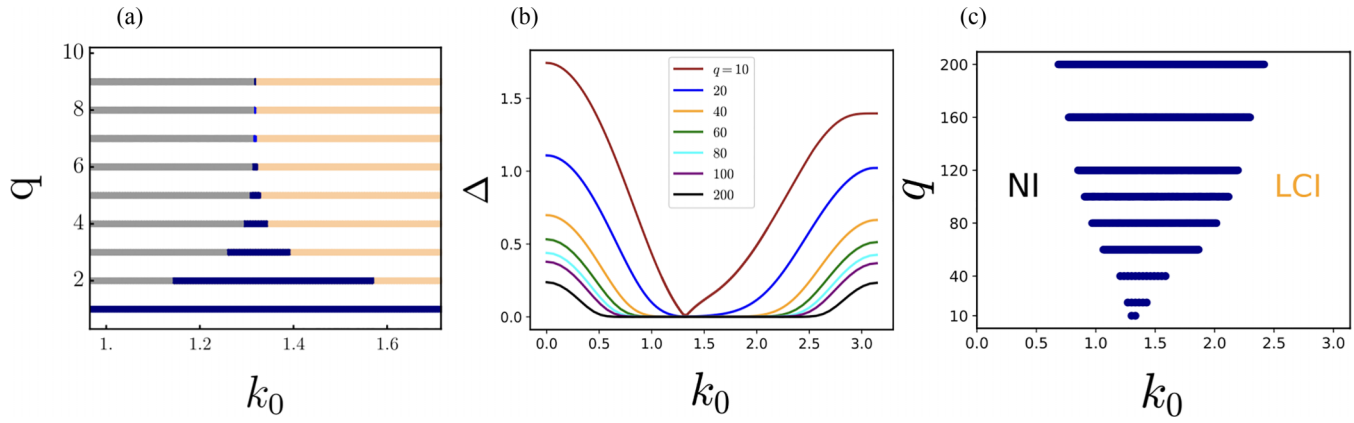

FIG. 2. (a) Phase diagram of the time-reversal broken WSM [Eq. (2)] with two WNs in presence of commensurate flux $\phi/\phi_0 = 1/q$ (magnetic flux quantum $\phi_0 = h/e$) per unit cell, for small q values (large fluxes) in the Hofstadter regime $l_B \sim a$. This phase diagram is obtained from the gapless solution of the Bloch-Hofstadter Hamiltonian Eq. (4). Here k_0 (in units of inverse lattice constant a) represents half the distance separating the two Weyl nodes of opposite chirality. The regions with grey, blue and orange color represent a normal insulator (NI), WSM and a LCI state respectively. (b) Energy gap Δ (in arbitrary unit) is plotted as a function of the separation parameter k_0 for large q values (small fluxes). (c) This phase diagram is derived with inputs from the Fig. 2(b). We notice a similarity between the two phase diagrams for the small and large q values (details in the text).

in flux, the WNs gradually converge within the magnetic BZ until, at a critical flux value, they meet and pairwise annihilate each other. This annihilation process leads to a smooth evolution of the surface Fermi arc. The direction in which the WNs approach each other depends on their initial separation $2k_0$: either towards the center or the boundary of the magnetic BZ. When the WNs converge towards the center, the surface Fermi arc fades away smoothly. Conversely, if they approach the boundary of the magnetic BZ, the surface Fermi arc of the WSM smoothly transitions into that of the LCI state.

B. Phase diagrams

The phase diagram, for a given flux $1/q$, can be obtained from the Eq. (7) by solving it for allowed k_0 values such that the right-hand side remains in the range $[-1, 1]$. The phase diagram is shown in Fig. 2(a) for small q values. There are two insulating regions in the phase diagram. We note that the gapless condition (7) is not enough to determine the nature of the two insulators in the phase diagram. We use numerics (to compute Chern numbers and surface states) to find the nature of the two insulators in the phase diagram. We will shortly see that a simple intuitive representation of pairwise annihilation of WNs by external fields can accurately predict the entire phase diagram including the nature of the insulators.

The WSM state, which existed for k_0 in the range $0 < k_0 < \pi$, now in an applied magnetic field exists in a smaller region [see Figs. 2(a) and 2(c)]. The WSM states with either small or large separation of WNs get gapped out first by the applied magnetic field and transform to insulators. The nature of the resulting insulators depends on the separation and the Fermi arc connectivity between the two WNs in the zero field model. In our model, the Fermi arc is an intra-BZ straight arc (along k_x) joining the projections of WNs of opposite chirality as shown in Fig. 1(a). We observe that a WSM state with small separation between the WNs produces a normal insulator, while a WSM state characterized by a large separation between the WNs gives rise to a layered Chern insulator (LCI) [41] after pairwise annihilation. The LCI state carries nonzero Chern numbers $C(k_x) = 1$ for all k_x values.

Let us take a closer look at the phase diagram Fig. 2(a) for small q values (large fluxes). We notice that as q is decreased, the region of the gapless WSM state expands. From physical point of view, this may seem counterintuitive because the magnetic length $l_B = \sqrt{\hbar/eB} = \sqrt{q}a$ (a lattice constant) decreases with decreasing q and hence we expect the region of the gapless WSM state in the phase diagram Fig. 2(a) to contract with decreasing q (recall pairwise annihilation occurs when $l_B \lesssim 1/k_0$). Actually, this behavior of the system for small q values (very large fluxes) in the Hofstadter regime $l_B \sim a$ is not contradictory but is consistent with what we expect in a lattice: The system should go towards the zero field limit as we decrease q because in the limit $q \to 1$, the phase factor $\exp(-i2\pi y_j p/q)$ (y_j is an integer) in the hopping term also approaches 1.

Now let us focus on higher q values (smaller fluxes) for which the magnetic length is much larger than the lattice constant. From the phase diagram Fig. 2(a), we see that the gapless region shrinks as magnetic flux is increased (or as q is decreased). From the gapless condition Eq. (7), we find that the gapless region actually shrinks almost to a point for q value as small as $q \sim 10$. This implies that for $q \gtrsim 10$ the transition from the normal insulator to the LCI state goes through a point instead of a region in the k_0 space. So the system remains gapless (WSM) only at the point $k_{0c} = r\frac{\pi}{2}$ ($r \approx 0.84$) for $q \gtrsim 10$.

This apparently means that an applied magnetic field with very large values of q i.e. an arbitrarily small field can destroy a WSM state with two WNs of arbitrary separation. From a physical point of view, an arbitrary small field cannot destroy a WSM state. There must be some additional information which is missing when we construct phase diagram from the gapless condition Eq. (7) only. A crucial information which is missing is that the energy gap (Δ), in the insulating states, falls exponentially [41] with increasing q (decreasing flux). Therefore to find the correct phase diagram for large values

of q in the regime $l_B \gg a$, we need to compute the energy gap Δ as a function of k_0 and q. We have computed the energy gap Δ numerically as a function of k_0 and plotted it for a series of values of q in Fig. 2(b). Now we find that the gapless WSM state exists in a finite region for a large value of $q = 200$. We also see that the gapless region contracts as we decrease the value of q from 200 to 100, 80, 60,...,10, which is according to our expectation: with decreasing q (increasing flux), the magnetic length $l_B = \sqrt{q}a$ decreases and hence the applied field annihilates a pair of WNs of higher and higher separation.

In summary, we find that the analytically obtained gapless condition produces correct phase diagram for small q values (very large fluxes) in the regime $l_B \sim a$. Since energy gap (in the insulating states) decreases exponentially with increasing q (decreasing flux), the gapless condition Eq. (7) is not enough to obtain correct phase diagram for large values of q in the regime $l_B \gg a$. For large values of q (smaller fluxes), we obtain phase diagram by computing the energy gap numerically.

C. An intuitive representation of pairwise annihilation process

We have observed that pairwise annihilation of WNs induced by external fields in a WSM with two WNs results in a normal insulator when WNs are closed spaced. However, a LCI state emerges when the separation between the two WNs is large. The above result can be understood through a simple picture based on the argument that a pair of WNs get annihilated when the inverse magnetic length l_B^{-1} becomes close to or larger than the separation $2k_0$ between the two Weyl nodes of opposite chirality. Note that in a periodic BZ, there are two separations between two WNs of opposite chirality located at $(k_0, 0, 0)$ and $(-k_0, 0, 0)$: (i) intra-BZ separation $2k_0$ and (ii) inter-BZ separation $2k_0' = 2\pi - 2k_0$. Clearly it is the shorter separation which determines how the pair will be annihilated by the applied field. Now consider a WSM with $k_0 < k_0'$. In this case, the inverse magnetic length l_B^{-1} will first reach $2k_0$. As magnetic field is increased, two WNs approach each other along the Fermi arc to meet at a point inside the BZ and get annihilated without leaving the Fermi arc (demonstrated in Fig. 1). This results in the formation of a normal insulator which possesses no surface states. On the other hand if $k_0 > k_0'$, the inverse magnetic length l_B^{-1} will first hit $2k_0'$ and consequently the pair of WNs is expected to get annihilated at the boundary of BZ by leaving the surface Fermi arc states. This results in a LCI state. The process is demonstrated in the Fig. 1. Note that the maximum separation occurs when $k_0 = \pi/2$ or $k_0' = \pi/2$. This implies that a very strong field is needed to destroy a WSM in which WNs are separated by a distance $2k_0 = \pi$. This is the reason why the WSM state survives in the central region of the phase diagram Fig. 2 in presence of an external magnetic field.

Here we want to point out that the region, in which the WSM state survives, shrinks with the increase in the strength of the field. At certain field values (around $q \sim 10$), this region contracts to a singular point. Based on the reasoning presented in the preceding paragraph, it is anticipated that this point is positioned at $k_0 = \pi/2$. On the contrary, in the model we have considered, the gapless region shrinks to the point $k_{0c} = r\frac{\pi}{2}$, $r \approx 0.84$, as mentioned earlier. It is important to note that we do not consider this value of k_{0c} to be universally applicable to all WSMs; rather, it may be contingent on specific yet unknown details of the considered model.

D. Pairwise annihilation in a WSM with multiple Weyl nodes

Examining pairwise annihilation becomes more challenging as the count of WNs rises because of a corresponding increase in the model's free parameters. Despite this complexity, the intuitive insights gained from studying pairwise annihilation in a WSM with two nodes can be readily extended to predict potential new states which can result in after pairwise annihilation in a WSM with multiple nodes. To illustrate let us consider a WSM with four Weyl nodes placed in a magnetic field which is aligned along the z direction. For simplicity, let us assume all the four Weyl nodes are located in the k_x-k_y plane at a constant $k_z = 0$, and they are at a maximum separation of π along the k_y direction. Clearly, maximum information about the location of the WNs are retained when they are projected on the k_x-k_y surface BZ. Projections of the WNs with an illustrative Fermi arc connectivity on the k_x-k_y surface BZ are depicted in Figs. 3(a) and 3(d). Since the WNs are located at the maximum separation along the k_y direction, the relevant separation parameters are k_{01} and k_{02} as shown in Fig. 3(a). Suppose $k_{02} > \pi/2$ and also $k_{02} \gg k_{01}$. Now if $k_{02}' < k_{01}$, then the magnetic length will first hit k_{02}'. In this situation as magnetic field is increased, the two WNs (separated by k_{02}) will approach each other across the BZ to meet at the boundary of the BZ. This results in pairwise annihilation of the two WNs (separated by k_{02}) by leaving the Fermi arc states. Thus we get a state with two WNs but with an additional surface Fermi arc [see Fig. 3(b)]. This state is a coexistent phase called W2′ which Ref. [41] found in a complicated model with many parameters. Now consider $k_{02}' > k_{01}$. In this case, the pairwise annihilation of the two WNs separated by k_{01} leads to a WSM state with only two Weyl nodes as demonstrated in Fig. 3(c).

Now it is clear that if $k_{01} = k_{02}$, then their pairwise annihilation by external magnetic fields would result either a normal insulator or an insulator (called I′) with counter propagating surface states as shown in Fig. 3(f).

For a magnetic field along the y direction, the separation parameters k_{01} and k_{02} are relevant only. In this case, the separation of the WNs along the k_y direction is completely irrelevant for pairwise annihilation of WNs. Hence, pairwise annihilation by magnetic fields aligned in the y direction would result in an identical set of phases as the previous case. We study this case in the Sec. III B in details.

The authors referenced in Ref. [41] explored an intricate model of a WSM featuring eight Weyl nodes. They successfully addressed the complexities of the multiparameter model and identified phases such as W2′ and I′ in the presence of a magnetic field. In our work, we have demonstrated how these phases could be derived from a simpler WSM model with only four Weyl nodes. Crucially, our approach does not rely on a particular model; instead, all that is necessary is knowledge of the WNs' positions and the Fermi arc connectivity in the surface BZ. This enables us to precisely predict the potential phases that may emerge in the presence of an external field.

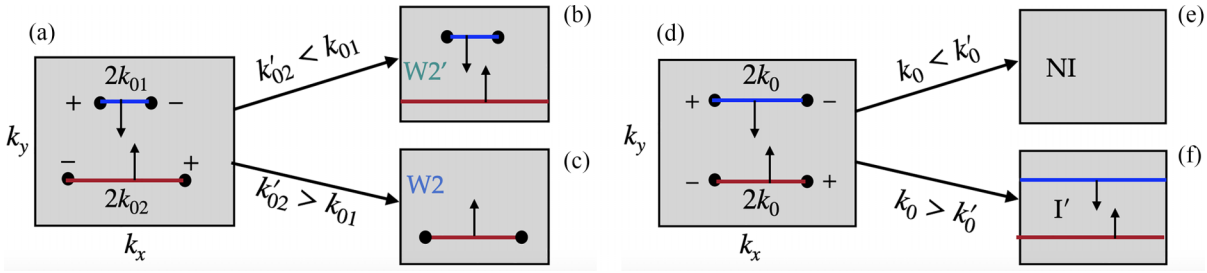

FIG. 3. An intuitive representation of pairwise annihilation process of WNs of opposite chirality by an external magnetic field. Figures (a) and (d) show the projections of the WNs (black dots) and the Fermi arcs on the k_x-k_y surface BZ. For a magnetic field aligned in the y-direction, separations of WNs along the k_x direction are relevant for pairwise annihilation. $2k_{01}$ and $2k_{02}$ are the intra-BZ separations and $2k'_{01} = 2\pi - 2k_{01}$ and $2k'_{02} = 2\pi - 2k_{02}$ are the corresponding inter-BZ separations. If $k'_{02} < k_{01}$, the pair of WNs separated by $2k_{02}$ will be annihilated at the boundary of BZ by leaving the Fermi arc states. Thus a coexistence phase W2′ emerges (see figure (b)). If $k'_{02} > k_{01}$, then the pair of WNs separated by $2k_{01}$ will be annihilated at some point inside the BZ without leaving the Fermi arcs. This results in a WSM (labelled W2) with two Weyl nodes (see (c)). Suppose $k_{01} = k_{02} = k_0$ as shown in (d). Now, it is clear that a normal insulator (NI) emerges when $k_0 < k'_0$, and an insulator (I′) with counter propagating surface states appears when $k_0 > k'_0$. Note that we would get the same set of phases if the magnetic field was aligned in the z direction, provided the separations of the WNs along the k_y direction is kept maximum.

E. Effect of Zeeman energy on the phase diagram

So far, we have completely ignored effect of Zeeman energy on the phase diagram. For a magnetic field along the z direction, the Zeeman term (H_Z) would be proportional to the σ_z i.e. $H_Z = E_Z\sigma_z$, where $E_Z \propto 1/q$. Addition of this term to the Hofstadter Hamiltonian Eq. (4), will modify only the quantity $f_3^\alpha(\mathbf{k}) \to f_3^\alpha(\mathbf{k}) + E_Z$. Therefore the band touching along the k_z direction will move from the point $k_{z0} = 0$ to $k_{z0} = \sin^{-1}(E_Z/t_z)$ (hopping along the z direction is parametrized by t_z). This change in band touching along the k_z direction flows to the quantity $f_1^\alpha(\mathbf{k})$ to cause a shift in the parameter k_0. The final result is that the critical point $k_0 = k_0^*$, at which a transition from WSM to insulator occurs, moves with the change in the Zeeman energy. Of course, this would not give any new phase but can move the phase boundary.

III. TIME-REVERSAL PRESERVED WSM

In the previous section, we have explored pairwise annihilation in a WSM with two Weyl nodes. A WSM with two WNs necessarily breaks time-reversal symmetry. In this section, we want to examine pairwise annihilation of WNs induced by external magnetic fields in a time-reversal preserved Weyl semimetals. A minimal model of time-reversal preserved WSM has four Weyl nodes. Now there will be two independent separation parameters (see Fig. 4). In Sec. II D, We have briefly looked at pairwise annihilation in a WSM with four WNs through an intuitive picture of pairwise annihilation. We restricted ourselves to a case where separation of the WNs along the k_y direction was fixed to simplify the analysis. We predicted emergence of an insulator, labeled I′, with counter propagating surface states [see Figs. 3(d)–3(f)]. Here we will verify this prediction. Below we explore pairwise annihilation in a WSM with four WNs in full details. The separations along both the k_x and k_y directions will be considered as free parameters in the theory.

To study pairwise annihilation of WNs in a time-reversal preserved WSM by external magnetic field whose strength can range all the way from small ($l_B \gg a$) to a very large value in the Hofstadter regime ($l_B \sim a$), we consider the following lattice model of WSM

$$H(\mathbf{k}) = (\cos k_2 - \cos k_y)\sigma_y + \sin k_z\sigma_z + (1 + \cos k_1 - \cos k_x - \cos k_z)\sigma_x, \tag{8}$$

with a minimal of four WNs located at $\mathbf{k}_{w_1} = (k_1, k_2, 0)$, $-\mathbf{k}_{w_1}$, $\mathbf{k}_{w_2} = (k_1, -k_2, 0)$, and $-\mathbf{k}_{w_2}$. They all lie in the same k_x-k_y plane at $k_z = 0$. The two Weyl nodes at $\mathbf{k}_{w_1}$ and $-\mathbf{k}_{w_1}$ are time-reversal partner of each other and they carry identical chiral charge $\chi = 1$. On the other hand the pair $\mathbf{k}_{w_2}$ and $-\mathbf{k}_{w_2}$ carries opposite chiral charge $\chi = -1$. The projections of the WNs with the Fermi arcs on the k_x-k_y surface BZ are depicted in the Fig. 4.

Here σ's, which are the two by two Pauli matrices, represent pseudo-spin degree of freedom. Time-reversal symmetry $\mathcal{T}H(\mathbf{k})\mathcal{T}^{-1} = H(-\mathbf{k})$ is realised by $\mathcal{T} = i\sigma_x\mathcal{K}$, where $\mathcal{K}$ acts by taking complex conjugation of any quantities appearing on the right of it.

Now we are ready to couple magnetic field to the Hamiltonian in Eq. (8) to study pairwise annihilation of WNs induced by the orbital field. Unlike the time-reversal broken model with two WNs, here in the time-reversal preserved model with

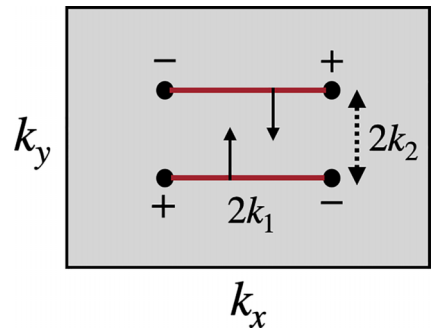

FIG. 4. Projections of the WNs and the Fermi arcs on the k_x-k_y surface BZ of the model in Eq. (8). The arrows indicate that the states on the two Fermi arcs are counter propagating. Clearly, there are two separations $2k_1$ and $2k_2$ between Weyl nodes of opposite chirality.

four WNs, the external magnetic field applied along any of the three axis direction can couple the WNs and can potentially annihilate them. The minimal model Eq. (8) has two free parameters k_1 and k_2 which provide separations of WNs of opposite chirality as shown in the Fig. 4. For magnetic field applied along the y direction (x direction), the separation parameter k_1 (k_2) is relevant only. This case is similar to the two WNs' problem where we had only one separation parameter. For magnetic field along the y direction, the intuitive picture of pairwise annihilation immediately tells that the new state which appears after pairwise annihilation is either a normal insulator or the insulator I′ with counter propagating surface states [see Fig. 3(f)]. We will verify our prediction by solving the model for phase diagrams in presence of an external commensurate magnetic field.

For magnetic field along the z direction, both the separation parameter plays significant role in pairwise annihilation of Weyl nodes. First, we solve this model for phase diagrams in presence of an external commensurate magnetic field along the z direction. Then, we argue that the phase diagrams can be derived, based on the intuitive picture of pairwise annihilation of WNs induced by external magnetic field.

A. Field along z direction

For a constant magnetic field $\mathbf{B} = B\hat{z}$, we can choose the Landau gauge $\mathbf{A} = (-y, 0, 0)B$ to work with. After going through same exercise as in Sec. II, we arrive at the following Hofstadter Hamiltonian:

$$H_\phi^{(z)} = \sum_{\mathbf{k}} \sum_{\alpha=0}^{q-1} c_\alpha^\dagger(\mathbf{k}) \big[f_1^\alpha(\mathbf{k})\sigma_x + f_2^\alpha(\mathbf{k})\sigma_y + f_3^\alpha(\mathbf{k})\sigma_z \big] c_\alpha(\mathbf{k}) - (c_{[\alpha+1]}^\dagger(\mathbf{k}) e^{iqk_y\delta_{(\alpha,q-1)}}\, T_y\, c_\alpha(\mathbf{k}) + \text{H.c.}) \tag{9}$$

for commensurate flux $\phi/\phi_0 = 1/q$ per unit cell. The functions $f_i^\alpha(\mathbf{k})$, $i = 1, 2, 3$ are given by

$$f_1^\alpha(\mathbf{k}) = 2\left(M - \cos\left(k_x + \frac{2\pi p}{q}\alpha \right) - \cos k_z \right), \tag{10a}$$

$$f_2^\alpha(\mathbf{k}) \equiv f_2(\mathbf{k}) = 2\cos k_2, \tag{10b}$$

$$f_3^\alpha(\mathbf{k}) \equiv f_3(\mathbf{k}) = 2\sin k_z, \tag{10c}$$

where $M = 1 + \cos k_1$ and the hopping matrix T_y in the second term of $H_\phi^{(z)}$ is $T_y = \sigma_y$. The Hamiltonian $H_\phi^{(z)}$ is to be diagonalized in the magnetic BZ: $k_x \in (0, 2\pi)$, $k_y \in (0, 2\pi/q)$, $k_z \in (0, 2\pi)$. We want to find all the gapless points in energy spectrum (band touching points) to construct the phase diagrams for different values of q. In the the basis $\Psi = (\psi_\uparrow, \psi_\downarrow)^T$, where $\psi_s = (c_{0,s}(\mathbf{k}), c_{1,s}(\mathbf{k}), \ldots, c_{q-1,s}(\mathbf{k}))^T$ and $s \equiv (\uparrow, \downarrow)$, the Hofstadter Hamiltonian $H_\phi^{(z)}$ can be expressed as $H_\phi^{(z)} = \sum_{\mathbf{k}} \Psi^\dagger(\mathbf{k}) h_\phi(\mathbf{k}) \Psi(\mathbf{k})$, where $h_\phi(\mathbf{k})$ (matrix of dimension $2q \times 2q$) has the following structure

$$h_\phi(\mathbf{k}) = \begin{pmatrix} \mathbf{A} & \mathbf{B} \\ \mathbf{C} & \mathbf{D} \end{pmatrix}, \tag{11}$$

where the diagonal blocks $\mathbf{A} = -\mathbf{D} = 2\sin k_z \mathbf{I}_q$ are proportional to identity $\mathbf{I}_q$ of dimension $q \times q$, and

$$\mathbf{B} = \begin{bmatrix} m_0 & u & 0 & 0 & \ldots & ue^{ik_y q} \\ u & m_1 & u & 0 & \ldots & 0 \\ 0 & u & m_2 & u & \ldots & \ldots \\ .. & .. & .. & .. & .. & .. \\ 0 & 0 & \ldots & u & m_{q-2} & u \\ ue^{-ik_y q} & 0 & \ldots & \ldots & u & m_{q-1} \end{bmatrix} = \mathbf{C}^\dagger. \tag{12}$$

Here $m_\alpha = f_1^\alpha(\mathbf{k}) - if_2^\alpha(\mathbf{k})$, $\alpha \in [0, q-1]$, and $u = -i$. We will refer the matrix $h_\phi(\mathbf{k})$ as the Bloch-Hofstadter Hamiltonian. The eigenvalues $E(\mathbf{k})$ (energy spectrum of the Hamiltonian $H_\phi^{(z)}$) of the Bloch-Hofstadter Hamiltonian are given by

$$\det \begin{bmatrix} \mathbf{A} - E(\mathbf{k})\mathbf{I}_q & \mathbf{B} \\ \mathbf{C} & \mathbf{D} - E(\mathbf{k})\mathbf{I}_q \end{bmatrix} = 0. \tag{13}$$

Since the diagonal blocks commutes with the off-diagonal blocks, the above condition reduces to

$$\det(\gamma \mathbf{I}_q - \mathbf{B}\mathbf{B}^\dagger) = 0, \tag{14}$$

where we have used $\tilde{\mathbf{A}}\tilde{\mathbf{D}} = \gamma \mathbf{I}_q$, $\gamma = E^2(\mathbf{k}) - (f_3(\mathbf{k}))^2$. Note that γ is the eigenvalue of the positive definite matrix $\mathbf{B}\mathbf{B}^\dagger$, so $\gamma \geqslant 0$. The energy spectrum is

$$E_n(\mathbf{k}) = \pm\sqrt{\gamma_n(q, \mathbf{k}) + (f_3(\mathbf{k}))^2}, \tag{15}$$

where $n = 1, 2, 3, \ldots q$, are the Landau level indices. Clearly the spectrum is symmetric about the zero energy. Therefore the gapless points between the highest occupied and lowest unoccupied bands are given by $E_1(\mathbf{k}) = 0$, which leads to two separate conditions $f_3(\mathbf{k}) = 2\sin k_z = 0$ and $\gamma_1(q, \mathbf{k}) = 0$. The first condition tells that band touching along the k_z direction can occur only at $k_{z0} = 0$ and/or π. Band touchings along the k_x and k_y directions can be found from Eq. (14) by setting $\gamma = 0$. Then Eq. (14) reduces to

$$\det(\mathbf{B}) = 0, \tag{16}$$

which is to be solved for a fixed q to find the k_x and k_y values at which band touching can occur. Analyzing the condition in Eq. (16), we find that $k_{z0} = \pi$ is not an allowed solution. Therefore band touching, if occurs in presence of magnetic field, along the k_z remains at $k_{z0} = 0$. For the case of the Hofstadter Hamiltonian in Eq. (4), a special form of the matrix $T_y = \sigma_x + i\sigma_y$ brought $\mathbf{B}$ in (almost) triangular form which made us possible to solve the above equation for arbitrary values of flux $1/q$. This is not the situation for the present case. Nevertheless we can make a progress for small q values, where the Eq. (16) can be solved by brute force. We have learned in Sec. II that the exact solution for the zeros of the Bloch-Hofstadter Hamiltonian produces correct phase diagram in the Hofstadter regime $l_B \sim a$ (i.e., small q values) only. For large q values (small fluxes) in the regime $l_B \gg a$, we construct the phase diagrams numerically by computing the energy gap as a function of the two parameters k_1 and k_2. Below we analytically compute the zeros of the Bloch-Hofstadter Hamiltonian to construct phase diagrams for small q values $q = 2,\ 3,\ 4$, and 5 only.

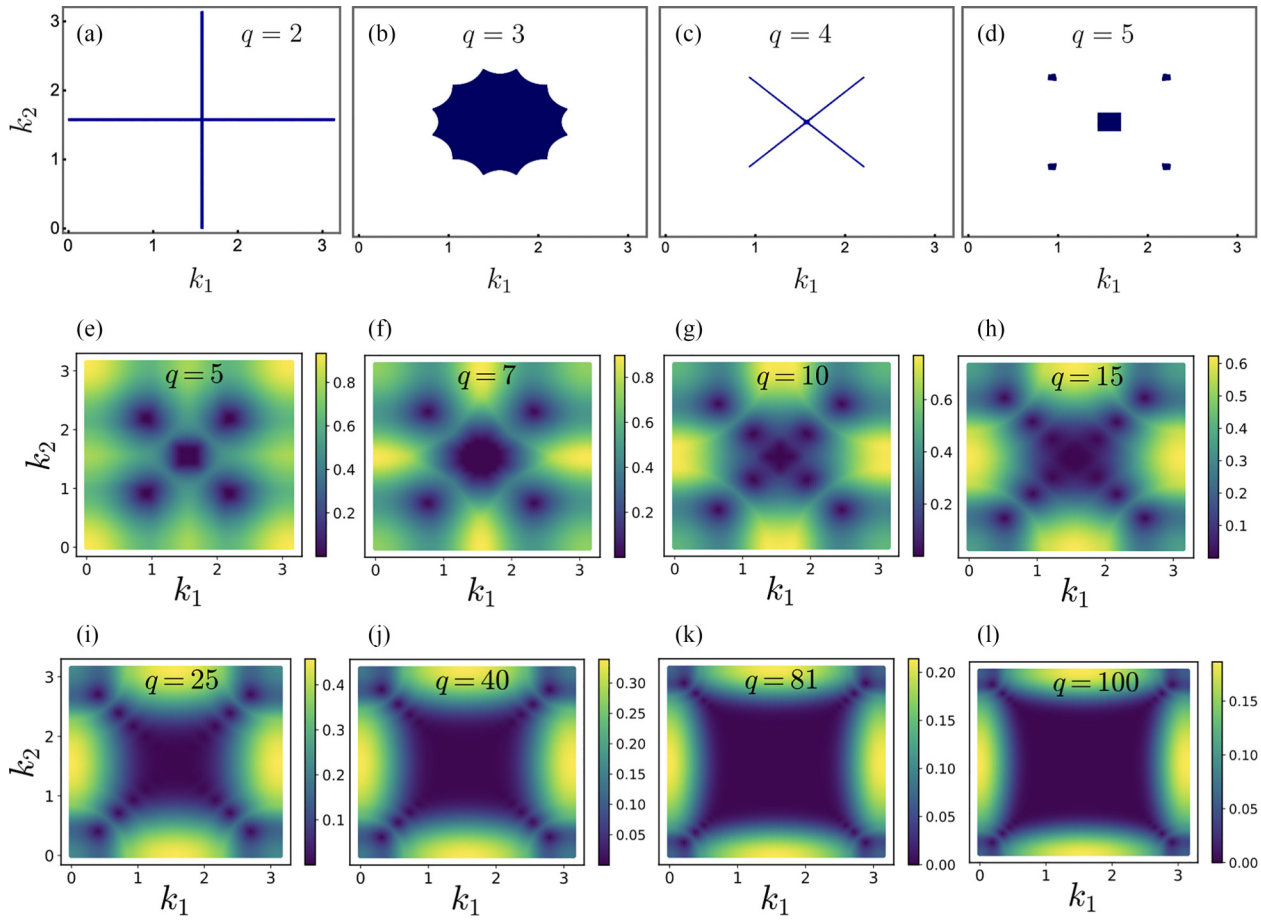

FIG. 5. Phase diagrams in Figs. 5(a)–5(d) for small $q = 2, 3, 4$, and 5 are obtained from the gapless (analytical) solutions of the Bloch-Hofstadter Hamiltonian Eq. (9). The dark-blue region(s) represent a gapless phase which is a WSM for $q = 3, 5$ (odd) and nodal line semimetal for $q = 2, 4$ (even). The white region represent a normal insulator. For larger q values (smaller fluxes), the phase diagrams can be derived by computing the energy gap as a function of the two separation parameters k_1 and k_2. The bulk energy gap (in arbitrary units) is computed numerically and plotted in Figs. 5(i)–5(l) for different values of flux $1/q$. The dark-blue regions represent a gapless phase. All the insulating regions (in yellow) are adiabatically connected. For large q value, say $q = 81$, we notice that the insulating regions appear where $|k_1 - \pi/2| \sim \pi/2$, $k_2 \sim \pi/2$ or $k_1 \sim \pi/2$, $|k_2 - \pi/2| \sim \pi/2$.

1. $q = 2$

Since the magnetic field is aligned along the z direction, band touching point along the k_z direction remains at $k_{z0} = 0$ for all q values. The corresponding k_x and k_y values for $q = 2$ are given by the condition

$$\det\begin{bmatrix} m_0 & u(1+e^{-iqk_y}) \\ u(1+e^{iqk_y}) & m_1 \end{bmatrix} = 0 \tag{17a}$$

$$m_0 m_1 - 2u^2(1+\cos qk_y) = 0, \tag{17b}$$

which can be simplified to a set of two conditions

$$\cos qk_x - \cos qk_y = 2(\cos^2 k_1 - \cos^2 k_2), \tag{18a}$$

$$\cos k_1 \cos k_2 = 0, \tag{18b}$$

We notice that the momenta k_x and k_y appear only in the first of the two conditions above. Therefore the gapless solution (if exists for some k_1 and k_2) describes a nodal line semimetal. The nodal line is located in the plane $k_z = 0$. The full gapless solution is shown as a shaded region in Fig. 5(a). The nodal line semimetal is not a stable phase. A small change in the parameters k_1 and k_2 immediately gaps out the state.

2. $q = 3$

Solving $\det(\mathbf{B}) = 0$ for $q = 3$, we get the following two conditions:

$$\cos qk_x = F_3(\cos k_1, \cos k_2), \tag{19a}$$

$$\cos qk_y = F_3(\cos k_2, \cos k_1), \tag{19b}$$

which k_x and k_y must satisfy in order to have gapless solution. The function $F_3(u, v) = 12uv^2 - 4u^3$. Recall that bands touching along the k_z direction can occur only at $k_{z0} = 0$. Therefore bands touching happens only at $k_{z0} = 0$ and the corresponding k_x, k_y values are determined by Eqs. 19(a) and 19(b). Clearly the solution space describes point touchings which are the Weyl points in the theory. A gapless solution exists in a finite region in the k_1-k_2 space as shown in Fig. 5(b). The full phase diagram consists of only two phases: a

topologically trivial insulating state and a gapless phase which is a WSM.

3. $q = 4$

Solving $\det(\mathbf{B}) = 0$ for $q = 4$, we get the following two conditions for bands touching:

$$\cos qk_x + \cos qk_y = 8(\cos^4 k_1 - 6\cos {k_1}^2 \cos^2 k_2 + \cos^4 k_2) + 2, \tag{20a}$$

$$\cos k_1 \cos k_2(\cos^2 k_1 - \cos^2 k_2) = 0. \tag{20b}$$

We notice that the k_x, k_y values, at which bands touching can occur, are solely determined by the first condition Eq. (21a) (provided the second condition is satisfied). The second condition, which involves only the two parameters k_1 and k_2 but no momenta, forces the gap closing to occur only on a contour (not a region) in the k_1, k_2 parameters space. Since the k_x, k_y values for bands touching are determined by only an one condition, the gapless solution describes nodal line semimetal. This is similar to what we have seen for the case of $q = 2$. The full phase diagram [depicted in Fig. 5(c)] consists of only two phases: a topologically trivial insulator and a gapless state which is a nodal line semimetal.

4. $q = 5$

Solving $\det(\mathbf{B}) = 0$ for $q = 5$, we get the following two conditions for a gapless solution:

$$\cos qk_x = F_5(\cos k_1, \cos k_2), \tag{21a}$$

$$\cos qk_y = F_5(-\cos k_2, \cos k_1), \tag{21b}$$

where $F_5(u, v) = 16u(u^4 - 10u^2v^2 + 5v^4) + 5u(1 + \sqrt{5})/2$. Similar to the case of $q = 3$, bands touching for $q = 5$ occurs at isolated points in the BZ: $k_z = 0$, and k_x, k_y values are given by the simultaneous solution of Eqs. (21a) and (21b). The band touching points are the Weyl points in the theory. Gapless solution exists in a finite region in the k_1-k_2 space as shown in Fig. 5(d). Like the phase diagram for $q = 3$, the phase diagram for $q = 5$ [see Fig. 5(d)] also consists of a WSM phase and a topologically trivial insulating phase only.

Finding gapless solution analytically becomes challenging as q increases. For $q > 5$, the phase digram can be understood by computing the energy gap as a function of k_1 and k_2. The result is shown in the second and third row of Fig. 5. We find that every insulating region is adiabatically connected, and all gapless regions characterize the same phase. For any odd values of $q = 1,\ 3,\ 5,\ 7,\ 9, \ldots$, the gapless regions describe a Weyl semimetal state. Though for small and even values of $q = 2,\ 4,\ 6, \ldots$, the gapless regions describe a nodal line semimetal state, for large values of q, the system, in the gapless regions, behaves like a WSM in terms of the low energy dispersion. When q is significantly large ($l_B \gg a$), it becomes challenging to differentiate the low energy spectra between even and odd values of q. As q increases, the energy bands along the k_x, k_y directions becomes flatter [41]. For large q values in the regime $l_B \gg a$ (semiclassical regime), the bands along the k_x, k_y directions become almost flat to form dispersionless Landau levels as expected from the continuum approximation in the semiclassical regime [17,44–46]. For an illustration, energy dispersion, for $q = 40$, along all the three k_x, k_y, k_z directions are depicted in Fig. 6.

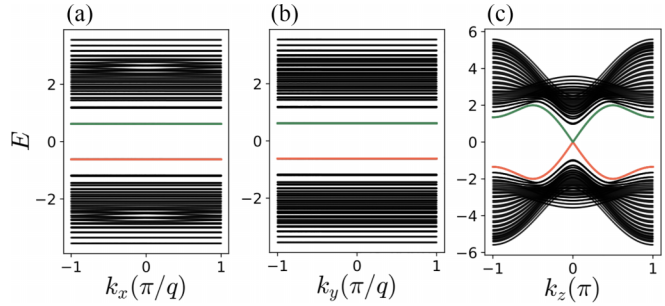

FIG. 6. Bulk energy dispersion E (in arbitrary units) of the Hofstadter Hamiltonian $H_\phi^{(z)}$, Eq. (9), for $q = 40$. The separation parameters are $k_1 = 2.0$ and $k_2 = 1.4$. For each of the plots, one of the momenta is allowed to vary, and the other ones are fixed at $k_x = 0.3\pi/q$, $k_y = 0.2\pi/q$ and $k_z = 0.1\pi$ appropriately. Energy bands along the k_x and k_y directions form flat Landau levels.

From the phase diagrams for large q values, we observe that the WSM state gets gapped out in some specific regions in the k_1-k_2 parameter space and the area of the insulating region increases with the strength of the applied magnetic field $|\mathbf{B}| \propto 1/q$. Let us closely examine the phase diagram for $q = 100$ [Fig. 5(l)], and focus on how the phase diagrams evolve as the value of q decreases.. We notice that regions, where $|k_1 - \pi/2| \sim \pi/2$ and $k_2 \sim \pi/2$ are gapped. Similarly, the regions where $k_1 \sim \pi/2$ and $|k_2 - \pi/2| \sim \pi/2$ are also gapped. However, the region in which $k_1 \sim \pi/2$ and $k_2 \sim \pi/2$ remains gapless (WSM). As q decreases [see Figs. 5(i) and 5(j)], the areas of the gapped insulating regions increase and simultaneously the areas of the gapless regions decrease. All these can be understood from the very fundamental concept that a pair of WNs of opposite chirality, which are separated by a momentum space distance $2k_0$, annihilates each other when the magnetic length $l_B = \sqrt{q}a$ hits the inverse separation $1/2k_0$. Clearly the regions with either small k_1 or small k_2 values will be gapped out first after pairwise annihilation of Weyl nodes. Recall when $k_1 > \pi/2$ or $k_2 > \pi/2$, one should compare the momentum space distances $k_1' = \pi - k_1$ and $k_2' = \pi - k_2$ with the inverse magnetic length. Therefore the regions with either $|k_1 - \pi/2| \sim \pi/2$ or $|k_2 - \pi/2| \sim \pi/2$ will be gapped out first. The separations between WNs of opposite chirality are maximum in the central region $k_1 \sim \pi/2$ and $k_2 \sim \pi/2$. This is the reason why it requires a very strong fields to gap out the central region.

An interesting tension occurs when $k_2 \approx k_1$ or $k_2 \approx \pi - k_1$. In this situation a single WN of chirality χ gets simultaneously coupled with two WNs of chirality $-\chi$. This leads to an effective coupling between two WNs of same chirality. Since a WN cannot annihilate another WN of same chirality, we get a partial annihilation of WNs along the line $k_2 \approx k_1$ or $k_2 \approx \pi - k_1$ in the phase diagrams.

What is common among all the phase diagrams is that there are only two phases: an insulator and a gapless state. Let us focus on a phase diagram for a particular value of $q = 40$. The entire insulating region in the phase diagram may be split into four subregions: left, right, top and bottom insulating regions. From the intuitive picture of pairwise

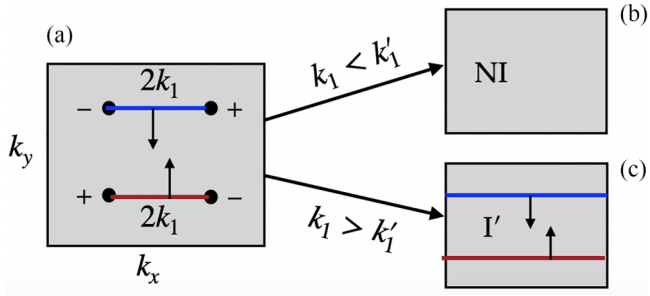

FIG. 7. (a) The Fermi arcs and the projections of the WNs on the k_x-k_y surface BZ of the WSM defined in Eq. (8). For magnetic field along y direction, the separation parameter k_1 is relevant for pairwise annihilation of Weyl nodes. If $k_1 < k_1'$, pairwise annihilation of the WMs, which occurs at a point inside the BZ, does not leave the Fermi arc states. Hence a normal insulator results in. If $k_1 > k_1'$, pairwise annihilation occurs at the boundary of the BZ by leaving the Fermi arc states. Hence, the insulator I′ emerges.

annihilation of WNs, we expect the insulators which are living in the left, top, and bottom regions will not have any surface states. The reason is the following. In the left region where $k_1 \ll \pi/2$ and $k_2 \sim \pi/2$, the separation parameter k_1 is relevant for pairwise annihilation. In this case, WNs which are separated by $2k_1$ get pairwise annihilated at some point inside the BZ. Hence no Fermi arc states are left. In the bottom region ($k_2 \ll \pi/2$) and top region ($k_2 \sim \pi$), the separation parameter k_2 is relevant for pairwise annihilation. Since the Fermi arcs are counter propagating, pairwise annihilation of WNs either at a point inside the BZ or at the boundary of the BZ cannot leave the Fermi arc states. We have verified this numerically. However, the insulator, which is living in the right insulating region where $k_1' \ll k_1$ and $k_2 \sim \pi/2$, can have surface states in accordance with our intuitive picture of pairwise annihilation of Weyl nodes (see Appendix for details). The bulk of this insulating state is of course trivial and the state is adiabatically connected to the adjacent insulating states.

B. Field along *y* direction

An external magnetic field oriented in the y direction cannot couple WNs which are separated along k_y direction. In this case, the crucial separation to consider for pairwise annihilation of WNs is k_1. The current problem can be thought of as a two copies of a two WNs' problem, similar to the time-reversal broken case studied in the Sec. II. Here, the separation parameter k_1 plays the role of the parameter k_0 of the time-reversal broken case [see Eq. (2)] with two Weyl nodes. The intuitive picture of pairwise annihilation of WNs [see Figs. 7 and also Figs. 3(d)–3(f)] immediately tells that the phase which appear after annihilation is either a normal insulator or an insulator (I′) with counter propagating surface states on the k_x-k_y surface BZ. In the following, we verify this prediction by solving the model for phase diagram in presence of commensurate magnetic fields.

We choose to work with the Landau gauge $\mathbf{A} = (z, 0, 0)B$. In this choice of gauge, the Hofstadter Hamiltonian takes the following form (after a unitary rotation in σ's space about the x direction)

$$H_\phi^{(y)} = \sum_{\mathbf{k}} \sum_{\alpha=0}^{q-1} c_\alpha^\dagger(\mathbf{k}) \left[f_1^\alpha(\mathbf{k})\sigma_x + f_3^\alpha(\mathbf{k})\sigma_z \right] c_\alpha(\mathbf{k}) - (c_{[\alpha+1]}^\dagger(\mathbf{k}) e^{iqk_z \delta_{(\alpha,q-1)}}\, T_z\, c_\alpha(\mathbf{k}) + \text{H.c.}), \tag{22}$$

for commensurate flux $\phi/\phi_0 = 1/q$ per unit cell. The functions $f_1^\alpha(\mathbf{k})$, $f_3^\alpha(\mathbf{k})$ are given by

$$f_1^\alpha(\mathbf{k}) = 2\left(M - \cos\left(k_x + \frac{2\pi}{q}\alpha \right) \right), \tag{23a}$$

$$f_3^\alpha(\mathbf{k}) \equiv f_3(\mathbf{k}) = 2(\cos k_2 - \cos k_y), \tag{23b}$$

where $M = 1 + \cos k_1$ and the hopping matrix $T_z = \sigma_x - i\sigma_y$. Note that the Hofstadter Hamiltonian $H_\phi^{(y)}$ is defined in the magnetic BZ: $k_x \in (0, 2\pi)$, $k_y \in (0, 2\pi)$, $k_z \in (0, 2\pi/q)$. We can obtain the phase diagrams by solving the spectrum for gapless points. Writing $H_\phi^{(y)}$ in a matrix form [same as Eq. (11)], we obtain $\mathbf{A} = -\mathbf{D} = 2(\cos k_2 - \cos k_y)\mathbf{I}_q$ and the block matrix $\mathbf{B}$ of the Bloch-Hofstadter Hamiltonian $h_\phi(\mathbf{k})$ is

$$\mathbf{B} = \begin{bmatrix} m_0 & -2 & 0 & 0 & \dots & 0 \\ 0 & m_1 & -2 & 0 & \dots & 0 \\ 0 & 0 & m_2 & -2 & \dots & \dots \\ .. & .. & .. & .. & .. & .. \\ 0 & 0 & \dots & 0 & m_{q-2} & -2 \\ 2e^{-iqk_z} & 0 & \dots & \dots & 0 & m_{q-1} \end{bmatrix}, \tag{24}$$

is almost an upper triangular matrix except the element $2e^{-ik_z q}$.

The quantity m_α, $\alpha = 0, 1, 2, \dots (q-1)$, is equal to $f_1^\alpha(\mathbf{k})$ i.e. $m_\alpha = f_1^\alpha(\mathbf{k})$. The Landau level energy spectrum is

$$E_n(\mathbf{k}) = \pm\sqrt{\gamma_n(q, \mathbf{k}) + (f_3(\mathbf{k}))^2}, \tag{25}$$

where $\gamma_n(q, \mathbf{k}) \geqslant 0$ are the eigenvalues of the positive definite matrix $\mathbf{B}\mathbf{B}^\dagger$, and $n = 1, 2, 3, \dots$ are the Landau level indices. Since the spectrum is symmetric about the zero energy, band touching points are given by the zero energy solutions. Clearly, for zero energy, we must have (i) $f_3(\mathbf{k}) = 2(\cos k_2 - \cos k_y) = 0$ and (ii) $\gamma_1(q, \mathbf{k}) = 0$. We see from the (i) condition that the band touching along the k_y direction remains at $k_{y0} = \pm k_2$ as we expected. The corresponding k_x and k_z values at which band touching can occur are determined by the (ii) condition. The condition (ii) tells that the determinant of the matrix $\mathbf{B}$ must vanish. Since $\mathbf{B}$ is almost an upper triangular, the determinant can be easily evaluated to be

$$\det(\mathbf{B}) = \prod_\alpha m_\alpha - 2^q e^{-iqk_z} = 2(T_q(g) - \cos qk_x) - 2^q e^{-iqk_z}, \tag{26}$$

where $T_q(g)$ is a Chebyshev polynomial of first kind of degree q, and $g = M = 1 + \cos k_1$. Setting $\det(\mathbf{B}) = 0$ and comparing its real and imaginary parts, we arrive at the following two conditions

$$\sin qk_z = 0, \tag{27a}$$

$$\cos qk_x = T_q(g) - 2^{q-1} \cos qk_z. \tag{27b}$$

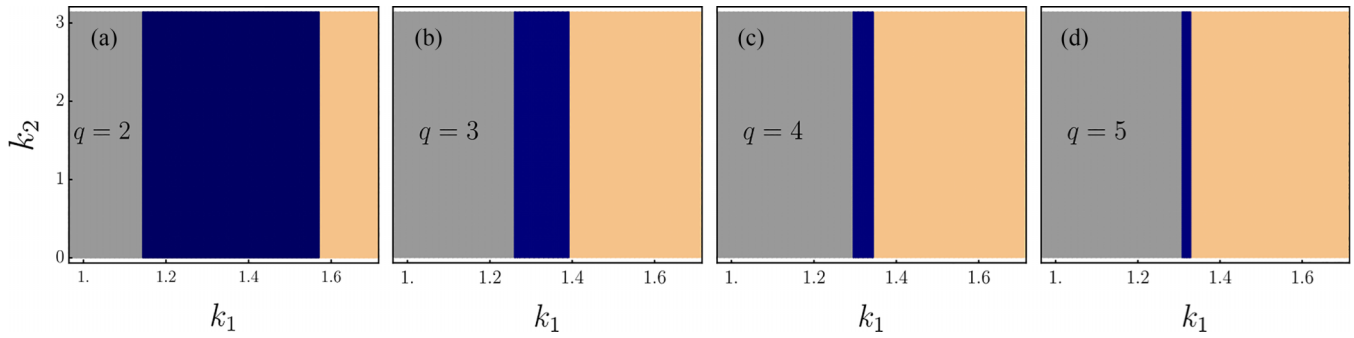

FIG. 8. Phase diagrams of the time-reversal preserved WSM [Eq. (8)] with four WNs in presence of $1/q$ commensurate flux per unit cell, along the y direction. k_1 and k_2 are the separation parameters (in units of the inverse lattice constant a) between Weyl nodes of opposite chirality. The shaded areas in grey, blue, and orange signify a normal insulator, Weyl semimetal, and an insulator (I′), respectively. The latter exhibits counterpropagating surface states along the open surface in the z direction.

The condition $\sin qk_z = 0$ gives two values of $k_{z0} = 0$ and π/q at which gap closing can happen. However, the solution $k_{z0} = \pi/q$ does not satisfy the condition Eq. (27b) because the right hand side of Eq. (27b) is always greater than the unity for all q's. Therefore band touching along the k_z direction remains at $k_z = 0$ and the corresponding k_x values are given by

$$\cos qk_x = T_q(g) - 2^{q-1}. \tag{28}$$

We notice that this condition is identical to the condition in Eq. (7) for the time-reversal broken case with two WNs, provided, we have made the replacement $k_0 \to k_1$. The above condition describe a region in the k_1 parameter's space for gapless solutions. The gapless phase describes the Weyl semimetal state. The full phase diagram is shown in Fig. 8 for multiple values of q. We notice that the phase diagrams are very similar to the phase diagrams of time-reversal broken case with two WNs. Now the WSM state has four WNs and the LCI state is to be replaced by the insulator I′ which has a pair of counter propagating Fermi arc surface states which are separated by a distance k_2 along the k_y direction in the k_x-k_y surface BZ. This confirms our prediction derived from the intuitive picture of pairwise annihilation: The phase which results in after pairwise annihilation by magnetic field aligned along the y direction is either a normal insulator or an insulator (I′) with counter propagating surface states on the k_x-k_y surface BZ.

C. Field along x direction

For magnetic field aligned along the x direction, the separation parameter k_2 is relevant for pairwise annihilation of Weyl nodes. We do not need to go through the whole calculation to find what would be the possible phases. We can easily guess the phase diagram from the intuitive picture of pairwise annihilation of Weyl nodes. In the zero field model, the Fermi arcs join projections of WPs which are separated along the k_x direction. Since the two Fermi arcs are counter propagating, the insulator which results in after pairwise annihilation of WNs either at a point inside the BZ or at the boundary of the BZ will be devoid of surface states. Therefore the phase diagram should consist of of two insulating regions (representing normal insulators which have no surface states) which are separated by a WSM phase in the central region.

IV. DISCUSSION

We have explored the minimal model of time-reversal broken and time-reversal preserved WSM with two and four WNs respectively to demonstrate how phase diagrams in presence of an external magnetic fields can be derived from an intuitive picture of pairwise annihilation of Weyl nodes. As the number of WNs increases, the complexity of solving the model to determine the phase diagram grows due to the escalating number of free parameters. The true strength of the intuitive representation of the pairwise annihilation process lies in its independence from intricate model details. It only necessitates information about the locations of WNs and Fermi arc connectivities in the surface BZ to predict the potential phases that may emerge after pairwise annihilation induced by magnetic fields.

Let us consider a WSM with six WNs and see if there is any new phase which was not there in the previous models with two and four Weyl nodes. Imagine all the WNs are located at the k_x-k_y plane at $k_z = 0$. Suppose the Fermi arcs connect the projection of WNs which are separated along the k_x direction as depicted in Fig. 9. Assume the magnetic field is applied along the y direction so that the separation k_1 and k_2 (as in Fig. 9) are relevant for pairwise annihilation. We have considered two scenarios. In the first scenario, we have $k_1 \ll \pi/2$ and $k_2 \sim \pi \to k_2' \ll \pi/2$. Now depending on the relative values of k_1 and k_2', the pairwise annihilation by magnetic field results in either an insulator (I′) or a new coexistent phase W2″. The second scenario, where we have $k_1 \sim \pi \to k_1' \ll \pi/2$ and $k_2 \ll \pi/2$, results in either a WSM state with two WNs or a new coexistence phase W4′. So we find that, in a WSM with six WNs, pairwise annihilation of WNs by external fields can lead to at least two new phases which were not possible in a WSM with two and four Weyl nodes.

We have seen that the pairwise annihilation of WNs by external field in a WSM results in a state which can be an insulator (e.g., NI, LCI, I′), a coexistence phase (e.g., W2′, W2″, W4′) or a WSM with reduced number of Weyl nodes. A pertinent question arises: are there any experimental signatures of these transitions? One potential quantity to investigate is the magnetoconductance. For example, the transition from a WSM state to a normal insulator can be distinguished from

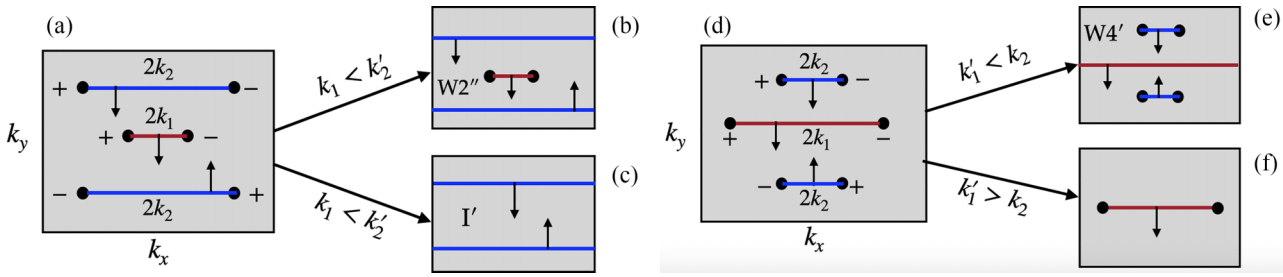

FIG. 9. An intuitive representation of pairwise annihilation of WNs by external magnetic field in a WSM with six Weyl nodes. Figures (a) and (d) depict the projections of the WNs (black dots) and the Fermi arcs in the k_x-k_y surface BZ. For a magnetic field aligned in the y-direction, only the two separation parameters k_1 and k_2 are relevant. In the first scenario (a), a coexistence phase W2″ emerges when $k_1 < k_2'$ [see (b)] and an insulator I′ with counter propagating surface states appear when $k_1 > k_2'$ [see (c)] after pairwise annihilation by magnetic fields. In the second scenario (d), pairwise annihilation results in either a coexistence phase W4′ or a WSM with two WNs, depending on the relative values of k_1' and k_2.

the transition of a WSM to a LCI state by measuring the magnetoconductance. Though, both the normal insulator and the LCI state are gapped in bulk, the LCI state has protected zero energy surface states. Suppose the WNs are at zero energy in the model (as we have in our case). There are no states available near zero energy in the normal insulating state to carry current. Therefore we expect the conductance, at the transition from the WSM state to the normal insulating state, to drop to zero. However, the conductance at the transition from the WSM to the LCI state should be finite because there are finite number of states near zero energy due to the zero energy surface states in the LCI state.

We have computed the (ballistic) magnetoconductance for the WSM model [Eq. (2)] with two Weyl nodes. The magnetic field is aligned along the z direction. The quantity of interest is G_{zz} which measures the longitudinal conductance along the z direction, i.e., along the direction of the applied magnetic field. We employ KWANT [47] simulation to compute the longitudinal conductance G_{zz}. The conductance G_{zz} is plotted in Fig. 10 for three different values of flux $1/q$. Because of the computational limitation arising due to the finite size of the system along the transverse directions (L_x and L_y), we restrict ourselves to only small q values. The chemical potential is fixed at $\mu = 0.1$. We clearly see that the conductance vanishes for small WNs separation (normal insulator) and it drops but remains finite for large WNs separation (LCI state). This demonstrates that the transition from a WSM state to a normal insulator may be distinguished from the transition of a WSM to a LCI state by measuring the longitudinal conductance in the experiment.

V. SUMMARY AND CONCLUSION

An external magnetic field, when aligned in the appropriate direction, can couple a pair of WNs of opposite chirality and can potentially annihilate the pair. Pairwise annihilation of WNs occurs when the inverse magnetic length l_B^{-1} becomes close to or larger than the momentum space separation $2k_0$ between the two WNs of opposite chirality. In this work, we have investigated pairwise annihilation of WNs by external magnetic field which ranges all the way from small ($l_B \gg a$) to a very large value in the Hofstadter regime ($l_B \sim a$). We have shown that pairwise annihilation of WNs by external magnetic field in a WSM with two WNs results in either a

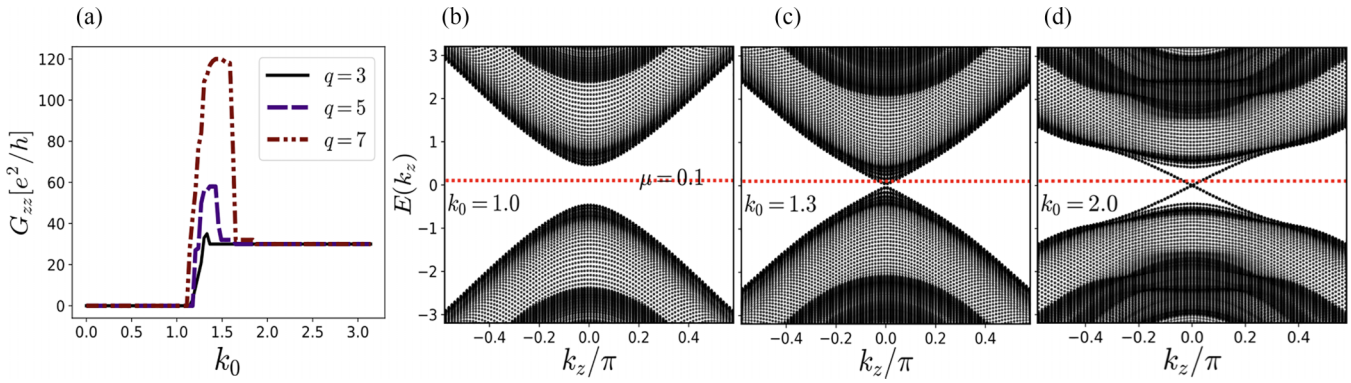

FIG. 10. (a) Longitudinal conductance G_{zz} as a function of separation parameter k_0 (in units of the inverse lattice constant a) between two WNs of opposite chirality for three different values of flux $1/q = 1/3, 1/5, 1/7$. Conductance is computed for a WSM slab of length $L_z = 100$ and width $L_x = L_y = 25$ [the model is defined in Eq. (2)]. The chemical potential is fixed at $\mu = 0.1$. The conductance G_{zz} is maximum for intermediate separation but vanishes for small separation and drops to finite value for large separation. (b)–(d) show the energy spectrum E (in arbitrary units) of the slab (taken periodic along the transport direction z) for three different values of $k_0 = 1.0$ (normal insulator), $k_0 = 1.3$ (WSM), and $k_0 = 2.0$ (LCI) for a fixed $q = 5$.

normal insulator or a layered Chern insulator. For a WSM with more than two WNs which are not collinear, the magnetic field which is applied along any of the three perpendicular directions can induce pairwise annihilation of Weyl nodes. The set of phases which appear for fields along, say, x direction is not identical to the set of phases for fields aligned in the z direction.

We conducted a comprehensive investigation into pairwise annihilation phenomena within both the time-reversal broken and time-reversal preserved models of WSMs. Our findings reveal that the pairwise annihilation of WNs induced by external magnetic fields leads to an emergence of a new state which can be an insulating state (e.g., NI, LCI, I′), a coexistence phase (e.g., W2′, W2″, W4′), or a WSM with a reduced number of Weyl nodes.

We have developed a model independent intuitive representation of pairwise annihilation process of WNs induced by external magnetic fields. This conceptual framework relies solely on information pertaining to the locations of the WNs and the connectivities of Fermi arcs on the surface BZ. With these essential inputs, our intuitive model accurately predicts the resulting phases following the pairwise annihilation of WNs induced by external magnetic fields.

This conceptual framework is versatile and can extend its applicability to elucidate the pairwise annihilation processes induced by external magnetic fields in other point node semimetals, such as three-dimensional Dirac semimetals, as well as two-dimensional point node semimetals such as Weyl semimetals and Dirac semimetals [48–55]. We anticipate further exploration of these systems in the future research.

ACKNOWLEDGMENTS

The author acknowledges the financial support provided by the Infosys Foundation. I wish to express my sincere thanks to ICTS for their warm hospitality during my visit, where a significant portion of this work was undertaken.

APPENDIX: THE INSULATING STATES DEPICTED IN THE PHASE DIAGRAMS ILLUSTRATED IN FIG. 5

In Sec. III, we have studied pairwise annihilation of WNs induced by external fields in a WSM with four Weyl nodes. All four WNs are located at the k_x-k_y plane at $k_z = 0$. Pairwise annihilation of WNs by magnetic field aligned in the z direction, results in a simple phase diagram as shown in Fig. 5. The phase diagram consists of only two phases: a gapless phase (WSM) and an insulator. Let us focus on a phase diagram for a particular value of $q = 100$ [Fig. 5(l)]. The entire insulating region in the phase diagram may be split into four subregions: left, right, top and bottom insulating regions. As we have argued in main text, the insulators which are living in the left, top and bottom regions will not have any surface states. However the insulator, which is living in the right insulating region where $k_1' \ll k_1$ and $k_2 \sim \pi/2$, can have surface states (in the k_x-k_y surface BZ) in accordance with our intuitive picture of pairwise annihilation process of Weyl nodes. The bulk of this insulating state is of course trivial and the state is adiabatically connected to the adjacent insulating states.

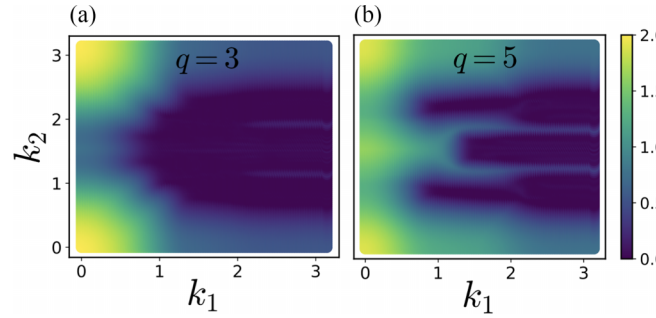

FIG. 11. Energy gap (in arbitrary units) of the system [Eq. (8)] in a slab geometry (finite along the z direction) is plotted as a function of the separation parameters k_1 and k_2. The slab has zero energy surface states in the dark-blue regions. Comparing with the phase diagrams Figs. 5(b) and 5(d), we see that the insulator which is living on the "right insulating region" has zero energy surface states. We take a representative point $k_1 = 2.6$, $k_2 = 2.2$ from the right insulating region for $q = 3$ to show the surface states in the Fig. 12.

We can numerically confirm whether the insulator living on the right insulating region has any zero energy surface states. Because of computational limitation, we do this for small values of $q = 3, 5$ (large q values require more computational resource). Note that even for small values of q, we can split the entire insulating regions into for subregions. The previous argument about existence of surface states for $q = 100$ also applies to the small values of q. Therefore we expect the insulator living on the "right insulating region" in the phase diagram for small values of q should have zero energy surface states. We have numerically computed energy gap of the system in a slab geometry (finite in the z direction) to look for the zero energy surface states. Since the spectrum of the Bloch-Hofstadter Hamiltonian is symmetric about the zero energy, we know for sure that the surface states (if exist) will be at the zero energy. The energy gap of the system in a slab geometry is plotted in Fig. 11. We can clearly see the insulator which is living on the right insulating region has zero energy surface states. The plots in the Fig. 12 show the zero energy surface states in the k_x-k_y surface BZ and the dispersion along the k_y direction.

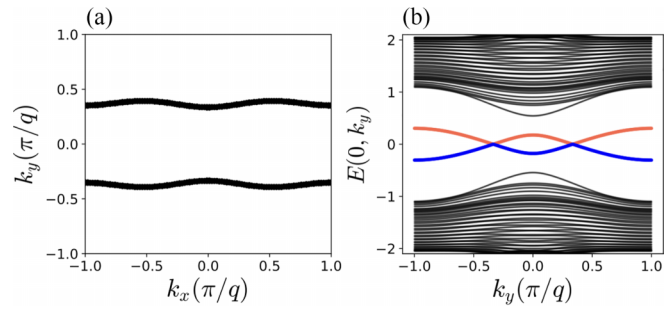

FIG. 12. (a) The zero energy surface states in the k_x-k_y surface BZ and (b) the dispersion along the k_y direction for $q = 3$ of the system [Eq. (8)] in a slab geometry (finite along the z direction). Values of the separation parameters are $k_1 = 2.6$, $k_2 = 2.2$, which represent a model for insulator [see Fig. 5(b)]. (b), the surface states, which lie in the bulk gap of the insulator, are highlighted.

[1] S. Murakami, Phase transition between the quantum spin Hall and insulator phases in 3D: emergence of a topological gapless phase, New J. Phys. **9**, 356 (2007).

[2] X. Wan, A. M. Turner, A. Vishwanath, and S. Y. Savrasov, Topological semimetal and fermi-arc surface states in the electronic structure of pyrochlore iridates, Phys. Rev. B **83**, 205101 (2011).

[3] K.-Y. Yang, Y.-M. Lu, and Y. Ran, Quantum Hall effects in a Weyl semimetal: Possible application in pyrochlore iridates, Phys. Rev. B **84**, 075129 (2011).

[4] A. A. Burkov and L. Balents, Weyl semimetal in a topological insulator multilayer, Phys. Rev. Lett. **107**, 127205 (2011).

[5] G. Xu, H. Weng, Z. Wang, X. Dai, and Z. Fang, Chern semimetal and the quantized anomalous Hall effect in $HgCr_2Se_4$, Phys. Rev. Lett. **107**, 186806 (2011).

[6] B. Q. Lv, H. M. Weng, B. B. Fu, X. P. Wang, H. Miao, J. Ma, P. Richard, X. C. Huang, L. X. Zhao, G. F. Chen, Z. Fang, X. Dai, T. Qian, and H. Ding, Experimental discovery of Weyl semimetal TaAs, Phys. Rev. X **5**, 031013 (2015).

[7] B. Q. Lv, N. Xu, H. M. Weng, J. Z. Ma, P. Richard, X. C. Huang, L. X. Zhao, G. F. Chen, C. E. Matt, F. Bisti, V. N. Strocov, J. Mesot, Z. Fang, X. Dai, T. Qian, M. Shi, and H. Ding, Observation of Weyl nodes in TaAs, Nat. Phys. **11**, 724 (2015).

[8] S.-Y. Xu, I. Belopolski, N. Alidoust, M. Neupane, G. Bian, C. Zhang, R. Sankar, G. Chang, Z. Yuan, C.-C. Lee, S.-M. Huang, H. Zheng, J. Ma, D. S. Sanchez, B. Wang, A. Bansil, F. Chou, P. P. Shibayev, H. Lin, S. Jia *et al.*, Discovery of a Weyl fermion semimetal and topological Fermi arcs, Science **349**, 613 (2015).

[9] S.-Y. Xu, N. Alidoust, I. Belopolski, Z. Yuan, G. Bian, T.-R. Chang, H. Zheng, V. N. Strocov, D. S. Sanchez, G. Chang, C. Zhang, D. Mou, Y. Wu, L. Huang, C.-C. Lee, S.-M. Huang, B. Wang, A. Bansil, H.-T. Jeng, T. Neupert *et al.*, Discovery of a Weyl fermion state with Fermi arcs in niobium arsenide, Nat. Phys. **11**, 748 (2015).

[10] L. Lu, Z. Wang, D. Ye, L. Ran, L. Fu, J. D. Joannopoulos, and M. Soljačić, Experimental observation of Weyl points, Science **349**, 622 (2015).

[11] H. Nielsen and M. Ninomiya, The Adler-Bell-Jackiw anomaly and Weyl fermions in a crystal, Phys. Lett. B **130**, 389 (1983).

[12] V. Aji, Adler-bell-jackiw anomaly in Weyl semimetals: Application to pyrochlore iridates, Phys. Rev. B **85**, 241101(R) (2012).

[13] A. A. Zyuzin and A. A. Burkov, Topological response in Weyl semimetals and the chiral anomaly, Phys. Rev. B **86**, 115133 (2012).

[14] D. T. Son and B. Z. Spivak, Chiral anomaly and classical negative magnetoresistance of Weyl metals, Phys. Rev. B **88**, 104412 (2013).

[15] E. V. Gorbar, V. A. Miransky, and I. A. Shovkovy, Chiral anomaly, dimensional reduction, and magnetoresistivity of Weyl and Dirac semimetals, Phys. Rev. B **89**, 085126 (2014).

[16] A. A. Burkov, Negative longitudinal magnetoresistance in Dirac and Weyl metals, Phys. Rev. B **91**, 245157 (2015).

[17] X. Li, B. Roy, and S. Das Sarma, Weyl fermions with arbitrary monopoles in magnetic fields: Landau levels, longitudinal magnetotransport, and density-wave ordering, Phys. Rev. B **94**, 195144 (2016).

[18] H.-Z. Lu and S.-Q. Shen, Quantum transport in topological semimetals under magnetic fields, Front. Phys. **12**, 127201 (2017).

[19] K. Das and A. Agarwal, Linear magnetochiral transport in tilted type-I and type-II Weyl semimetals, Phys. Rev. B **99**, 085405 (2019).

[20] K. Das, S. K. Singh, and A. Agarwal, Chiral anomalies induced transport in Weyl metals in quantizing magnetic field, Phys. Rev. Res. **2**, 033511 (2020).

[21] P. Fontana, M. Burrello, and A. Trombettoni, Topological van hove singularities at phase transitions in Weyl metals, Phys. Rev. B **104**, 195127 (2021).

[22] S. Nandy, G. Sharma, A. Taraphder, and S. Tewari, Chiral anomaly as the origin of the planar Hall effect in Weyl semimetals, Phys. Rev. Lett. **119**, 176804 (2017).

[23] H. Li, H.-W. Wang, H. He, J. Wang, and S.-Q. Shen, Giant anisotropic magnetoresistance and planar Hall effect in the Dirac semimetal Cd_3As_2, Phys. Rev. B **97**, 201110(R) (2018).

[24] Shama, R. Gopal, and Y. Singh, Observation of planar Hall effect in the ferromagnetic Weyl semimetal $Co_3Sn_2S_2$, J. Magn. Magn. Mater. **502**, 166547 (2020).

[25] L. Li, J. Cao, C. Cui, Z.-M. Yu, and Y. Yao, Planar Hall effect in topological Weyl and nodal-line semimetals, Phys. Rev. B **108**, 085120 (2023).

[26] Y.-W. Wei, J. Feng, and H. Weng, Spatial symmetry modulation of planar Hall effect in Weyl semimetals, Phys. Rev. B **107**, 075131 (2023).

[27] A. C. Potter, I. Kimchi, and A. Vishwanath, Quantum oscillations from surface fermi arcs in Weyl and Dirac semimetals, Nat. Commun. **5**, 5161 (2014).

[28] Y. Zhang, D. Bulmash, P. Hosur, A. C. Potter, and A. Vishwanath, Quantum oscillations from generic surface fermi arcs and bulk chiral modes in Weyl semimetals, Sci. Rep. **6**, 23741 (2016).

[29] P. J. W. Moll, N. L. Nair, T. Helm, A. C. Potter, I. Kimchi, A. Vishwanath, and J. G. Analytis, Transport evidence for fermi-arc-mediated chirality transfer in the Dirac semimetal Cd_3As_2, Nature (London) **535**, 266 (2016).

[30] C. M. Wang, H.-P. Sun, H.-Z. Lu, and X. C. Xie, 3d quantum Hall effect of fermi arcs in topological semimetals, Phys. Rev. Lett. **119**, 136806 (2017).

[31] C. Zhang, Y. Zhang, X. Yuan, S. Lu, J. Zhang, A. Narayan, Y. Liu, H. Zhang, Z. Ni, R. Liu, E. S. Choi, A. Suslov, S. Sanvito, L. Pi, H.-Z. Lu, A. C. Potter, and F. Xiu, Quantum Hall effect based on Weyl orbits in Cd_3As_2, Nature (London) **565**, 331 (2019).

[32] H. Li, H. Liu, H. Jiang, and X. C. Xie, 3d quantum Hall effect and a global picture of edge states in Weyl semimetals, Phys. Rev. Lett. **125**, 036602 (2020).

[33] M. Chang, H. Geng, L. Sheng, and D. Y. Xing, Three-dimensional quantum Hall effect in Weyl semimetals, Phys. Rev. B **103**, 245434 (2021).

[34] R. Ma, D. N. Sheng, and L. Sheng, Three-dimensional quantum Hall effect and magnetothermoelectric properties in Weyl semimetals, Phys. Rev. B **104**, 075425 (2021).

[35] M. Chang, Y. Ge, and L. Sheng, Generalization of the theory of three-dimensional quantum Hall effect of Fermi arcs in Weyl semimetal, Chin. Phys. B **31**, 057304 (2022).

[36] X.-X. Zhang and N. Nagaosa, Anisotropic three-dimensional quantum Hall effect and magnetotransport in mesoscopic Weyl semimetals, Nano Lett. **22**, 3033 (2022).
[37] P. Kim, J. H. Ryoo, and C.-H. Park, Breakdown of the Chiral anomaly in Weyl semimetals in a strong magnetic field, Phys. Rev. Lett. **119**, 266401 (2017).
[38] C.-K. Chan and P. A. Lee, Emergence of gapped bulk and metallic side walls in the Zeroth landau Level in Dirac and Weyl semimetals, Phys. Rev. B **96**, 195143 (2017).
[39] C.-L. Zhang, S.-Y. Xu, C. M. Wang, Z. Lin, Z. Z. Du, C. Guo, C.-C. Lee, H. Lu, Y. Feng, S.-M. Huang, G. Chang, C.-H. Hsu, H. Liu, H. Lin, L. Li, C. Zhang, J. Zhang, X.-C. Xie, T. Neupert, M. Z. Hasan *et al.*, Magnetic-tunnelling-induced Weyl node annihilation in Tap, Nat. Phys. **13**, 979 (2017).
[40] B. J. Ramshaw, K. A. Modic, A. Shekhter, Y. Zhang, E.-A. Kim, P. J. W. Moll, M. D. Bachmann, M. K. Chan, J. B. Betts, F. Balakirev, A. Migliori, N. J. Ghimire, E. D. Bauer, F. Ronning, and R. D. McDonald, Quantum limit transport and destruction of the Weyl nodes in TaAs, Nat. Commun. **9**, 2217 (2018).
[41] F. Abdulla, A. Das, S. Rao, and G. Murthy, Time-reversal-broken Weyl semimetal in the Hofstadter regime, SciPost Phys. Core **5**, 014 (2022).
[42] R. Peierls, Zur theorie des diamagnetismus von leitungselektronen, Z. Phys. **80**, 763 (1933).
[43] D. R. Hofstadter, Energy levels and wave functions of bloch electrons in rational and irrational magnetic fields, Phys. Rev. B **14**, 2239 (1976).
[44] M. O. Goerbig, J.-N. Fuchs, G. Montambaux, and F. Piéchon, Tilted anisotropic Dirac cones in quinoid-type graphene and $\alpha-(\mathrm{BEDT\text{-}TTF})_2\mathrm{I}_3$, Phys. Rev. B **78**, 045415 (2008).
[45] A. A. Burkov, M. D. Hook, and L. Balents, Topological nodal semimetals, Phys. Rev. B **84**, 235126 (2011).
[46] S. Tchoumakov, M. Civelli, and M. O. Goerbig, Magnetic-field-induced relativistic properties in type-I and type-II Weyl semimetals, Phys. Rev. Lett. **117**, 086402 (2016).
[47] C. W. Groth, M. Wimmer, A. R. Akhmerov, and X. Waintal, Kwant: a software package for quantum transport, New J. Phys. **16**, 063065 (2014).
[48] S. M. Young and C. L. Kane, Dirac semimetals in two dimensions, Phys. Rev. Lett. **115**, 126803 (2015).
[49] J. Kim, S. S. Baik, S. W. Jung, Y. Sohn, S. H. Ryu, H. J. Choi, B.-J. Yang, and K. S. Kim, Two-dimensional Dirac fermions protected by space-time inversion symmetry in black phosphorus, Phys. Rev. Lett. **119**, 226801 (2017).
[50] Y. J. Jin, B. B. Zheng, X. L. Xiao, Z. J. Chen, Y. Xu, and H. Xu, Two-dimensional Dirac semimetals without inversion symmetry, Phys. Rev. Lett. **125**, 116402 (2020).
[51] X. Feng, J. Zhu, W. Wu, and S. A. Yang, Two-dimensional topological semimetals, Chin. Phys. B **30**, 107304 (2021).
[52] W. Meng, X. Zhang, Y. Liu, L. Wang, X. Dai, and G. Liu, Two-dimensional Weyl semimetal with coexisting fully spin-polarized type-I and type-II Weyl points, Appl. Surf. Sci. **540**, 148318 (2021).
[53] T. He, X. Zhang, Y. Liu, X. Dai, G. Liu, Z.-M. Yu, and Y. Yao, Ferromagnetic hybrid nodal loop and switchable type-I and type-II Weyl fermions in two dimensions, Phys. Rev. B **102**, 075133 (2020).
[54] J.-Y. You, C. Chen, Z. Zhang, X.-L. Sheng, S. A. Yang, and G. Su, Two-dimensional Weyl half-semimetal and tunable quantum anomalous Hall effect, Phys. Rev. B **100**, 064408 (2019).
[55] F. Abdulla, Protected Weyl semimetals within 2d chiral classes, arXiv:2401.04656.